

that even under severe selective pressure, microbial life in the Antarctic has been unable to discover a comparable mechanism. To some, this may suggest that life on Mars is an impossibility. In view of the very different histories of Mars and the dry valleys, including the recent age ( $10^4$  to  $10^5$  years) of the latter, and the obvious uncertainties concerning the metabolic potentialities of extraterrestrial life forms, we believe that such a conclusion is not justified. The findings suggest, however, that martian life could not be built on a terrestrial model.

Finally, the Antarctic has provided us with a natural environment as much like Mars as any we are likely to find on Earth. In this environment, the capacity of life as we know it to adapt and survive is pushed to its limit. The concentration of living things around the sources of water in the dry valleys and their rapid thinning out in the most arid locales may be useful as a model of the distribution of the life we may, if we are lucky, find on Mars.

#### References and Notes

1. R. E. Cameron, in *Arid Lands in Perspective*, W. G. McGinnies and B. J. Goldman, Eds. (Univ. of Arizona Press, Tucson, 1969), p. 169.
2. ———, J. King, C. N. David, in *Antarctic Ecology*, M. W. Holdgate, Ed. (Academic Press, New York, 1970), p. 702; R. E. Cameron, in *Research in the Antarctic*, L. O. Quam and H. D. Porter, Eds. (AAAS, Washington, D.C., 1971), p. 137.
3. N. H. Horowitz, A. J. Bauman, R. E. Cameron, P. J. Geiger, J. S. Hubbard, G. P. Shulman, P. G. Simmonds, K. Westberg, *Science* **164**, 1054 (1969).
4. R. E. Cameron and H. P. Conrow, *Antarct. J.* **4**, 28 (1969); R. E. Cameron and E. L. Merek, *Technical Report 32-1522* (Jet Propulsion Laboratory, California Institute of Technology, Pasadena, 1971).
5. R. E. Cameron, C. N. David, J. King, *Antarct. J.* **3**, 164 (1968).
6. M. J. Rubin and W. S. Weyant, in *Antarctica*, T. Hatherton, Ed. (Praeger, New York, 1965), p. 375.
7. C. Bull, *Antarct. Res. Ser.* **9**, 177 (1966).
8. R. L. Nichols, *Amer. J. Sci.* **261**, 20 (1963).
9. A. T. Wilson, in *Antarctic Ecology*, M. W. Holdgate, Ed. (Academic Press, New York, 1970), p. 21.
10. P. E. Calkin, *Institute of Polar Studies Report No. 10* (Institute of Polar Studies, Ohio State University, Columbus, 1964).
11. T. Torii and J. Osaka, *Science* **149**, 975 (1965).
12. *Handbook of Chemistry and Physics, 49th Edition* (Chemical Rubber Co., Cleveland, 1968), p. E-37.
13. G. G. C. Claridge and I. B. Campbell, *Nature* **217**, 428 (1968); G. Mueller, *ibid.* **219**, 1131 (1968).
14. A. P. Ingersoll, *Science* **168**, 972 (1970).
15. E. C. Dougherty and L. G. Harris, *Science* **140**, 497 (1963).
16. W. L. Boyd, J. T. Staley, J. W. Boyd, *Antarct. Res. Ser.* **8**, 125 (1966).
17. R. E. Benoit and C. E. Hall, Jr., in *Antarctic Ecology*, M. W. Holdgate, Ed. (Academic Press, New York, 1970), p. 697.
18. R. E. Cameron, unpublished data.
19. G. V. Levin, *Advan. Appl. Microbiol.* **10**, 55 (1968).
20. J. S. Hubbard, unpublished data.
21. ———, G. L. Hobby, N. H. Horowitz, P. J. Geiger, F. A. Morelli, *Appl. Microbiol.* **19**, 32 (1970).
22. J. J. Skujins, in *Soil Biochemistry*, A. D. McLaren and G. H. Peterson, Eds. (Dekker, New York, 1967), p. 371.
23. G. H. Peterson, *Soil Sci.* **94**, 71 (1962).
24. C. L. Hall, thesis, Virginia Polytechnic Institute (1968).
25. G. H. Meyer, M. B. Morrow, O. Wyss, T. E. Berg, J. L. Littlepage, *Science* **138**, 1103 (1962).
26. R. E. Cameron and J. S. Hubbard, unpublished data.
27. R. E. Benoit and R. E. Cameron, paper presented at the 67th annual meeting of the American Society for Microbiology in New York, 1967.
28. G. H. Lacy, personal communication.
29. W. J. Scott, *Advan. Food Res.* **7**, 83 (1957).
30. This article presents the results of one phase of research carried out at the Jet Propulsion Laboratory, California Institute of Technology, Pasadena, under NASA contract NAS 7-100. Logistic support and facilities for the Antarctic part of this study were provided by the Office of Antarctic Programs of the National Science Foundation under contract C-585. We thank H. Conrow, D. Gensel, A. Miller, and F. Morelli for valuable assistance.

## Electron Spectroscopy with Monochromatized X-rays

This technique constitutes a second-generation approach for a new analytical method.

K. Siegbahn, D. Hammond, H. Fellner-Feldegg, E. F. Barnett

In recent years electron spectroscopy for chemical analysis (ESCA) has been developed to the point where it promises to be of considerable importance to the chemist. In electron spectroscopy the sample to be studied is irradiated with x-ray or ultraviolet radiation. The sample emits electrons, which may be photoelectrons or Auger electrons. The energy spectra of these electrons are then analyzed in a high-resolution magnetic or electrostatic spectrometer. The nature of the resulting spectrum depends on the type of excitation used.

In the initial work in electron spec-

troscopy x-ray excitation was used (1, 2). The energy of the photoelectrons is equal to the energy of the incident photons minus the binding energy. Hence, the electronic energy levels of elements present in the sample can be determined directly and with great precision. All elements except hydrogen have core electrons whose energy levels are characteristic of the element even when it is combined with other elements to form complex molecular compounds. Sufficient sensitivity can be attained so that elements can be detected and studied even if they constitute only a small

fraction of the sample material. Measurement of the relative intensities of spectral lines from different elements in a compound yields quantitative information about its composition. With an appropriate calibration (taking care of the variation in photoelectric yield with atomic number and other factors), quantitative analysis can be carried out with an accuracy of a few percent.

The electronic states are modified by the molecular environment of the atom. The amount of structural information that can be obtained by measuring the chemical shift of electrons in the core levels is limited in many cases by the resolution of the available instrumentation. We describe here some recent developments that have resulted in improved resolution based on crystal monochromatization of the x-rays.

For a solid sample, the electrons which form the ESCA spectrum come from a very thin layer near the surface, typically less than 50 angstroms in depth, with the depth of the layer depending on the energy of the photoelectron and the material. The method is therefore useful for the study of surface phenomena. The sensitivity attainable is such that a spectrum can be

Dr. Siegbahn is head of the Institute of Physics, University of Uppsala, Uppsala, Sweden; Mr. Hammond and Dr. Fellner-Feldegg are with Hewlett-Packard Laboratories, Palo Alto, California 94304; Mr. Barnett was associated with Hewlett-Packard Laboratories until his death on 8 August 1971.

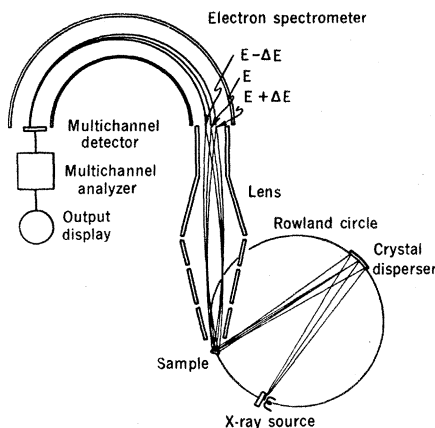


Fig. 1. Schematic drawing of the ESCA spectrometer based on the use of x-ray monochromatization and dispersion compensation.

obtained with a fraction of an atomic layer.

Samples that are condensable gases or liquids with high vapor pressures at room temperature can be handled by cryogenic freezing. Extensive work has also been done on gaseous samples; in these cases the gas sample is at a pressure of the order of 1 torr. The sample is separated from the high vacuum of the spectrometer ( $\sim 10^{-6}$  torr) by a set of differentially pumped apertures which permit the photoelectrons to pass through (2).

Electron spectroscopy with excitation by ultraviolet radiation has been extensively developed in recent years (3). This technique has been used for the investigation of low-lying (valence band) states. Because the incident radiation is more monochromatic and the energy resolution is higher for low-energy ultraviolet radiation than for x-radiation, detailed analysis is possible. Most work has been done with helium resonance radiation having photon energies of 21 and 40.8 electron volts. If the sample is in the gaseous state, energy levels can be measured with a resolution of 10 to 25 millielectron volts. Solids, however, have broader lines and this limits the obtainable resolution.

## History

Early experiments in photoelectron spectroscopy did not reveal any sharp electron lines, primarily because of the relatively low resolution of the electron spectrometers then available. The energy lost by photoelectrons before they emerge from the irradiated sample was generally assumed to be the limiting factor. Electron binding energies could

be determined from the positions of the edges of the emission lines in the photoelectron spectrum. However, this method did not compete in accuracy with x-ray absorption spectroscopy, and it was little used for many years.

In connection with studies in nuclear physics, in the early 1950's an iron-free, magnetic, double-focusing electron spectrometer with improved resolution was developed. With this instrument extremely sharp lines in the photoelectron spectra could be observed. The width of each of these lines is dependent on the inherent width of the atomic levels and the characteristic x-radiation. These lines were shown to consist of electrons that had emerged from the sample without energy loss. Their energy was, therefore, equal to the difference between the energy of the incident x-ray photon and the binding energy of the electron. From measurements of the kinetic energies of these electrons the electron binding energies could then be determined with much greater accuracy and simplicity than could be attained with x-ray absorption spectroscopy or any other known method. Other types of spectroscopy yield information about the difference between energy levels, whereas ESCA measurements provide direct information about the absolute energy levels.

In all the work reported before 1966 the x-rays were not filtered in any way before striking the sample. As a result the interpretation of the electron spectra was complicated by the presence of the bremsstrahlung background and other x-ray emission lines in the x-ray spectrum. Each emission line produces its own ESCA spectrum. More important, the inherent widths of the emission lines (typically of the order of 1 electron volt) limit the resolution attainable. The inherent widths of the atomic energy levels range from approximately 0.1 electron volt for light elements to 10 electron volts or more for the inner levels of heavy elements (4). However, as ESCA measurements have shown, even heavy elements have outer levels with inherent widths of not more than a few tenths of an electron volt (1). Thus, in many cases the intrinsic line width is not reached, so that an improvement in system resolution is desirable. Greater resolution is also needed because the x-ray line width of  $\sim 1.0$  electron volt is not negligible as compared with the total range of chemical shifts which is typically 10 electron volts. Methods of using a monochromator to eliminate the contribution of the x-ray line width to

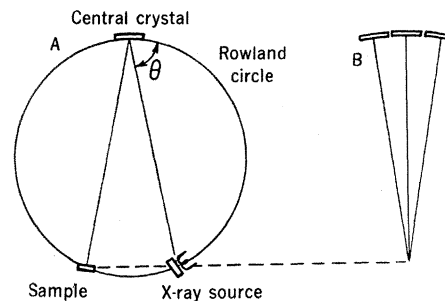


Fig. 2. X-ray monochromator.

the electron line width have been described (1, 2).

In the first ESCA experiments incorporating a crystal monochromator, a cylindrically bent crystal and photographic detection were used (5). With this system the predicted advantages of freedom from satellite lines and bremsstrahlung background were demonstrated. In this article we report the achievement of the predicted advantage of improved resolution through monochromatization of the x-rays brought about by the use of a spherically bent crystal. The system incorporates the principle of dispersion compensation (which will be discussed below) to give high resolution while preserving sensitivity.

## Design Principles

The four basic elements of a dispersion-compensated ESCA system are the monochromator, the electron lens, the electron spectrometer, and the multichannel detection system. These components interact as shown schematically in Fig. 1. X-rays from an aluminum anode are dispersed by a bent crystal

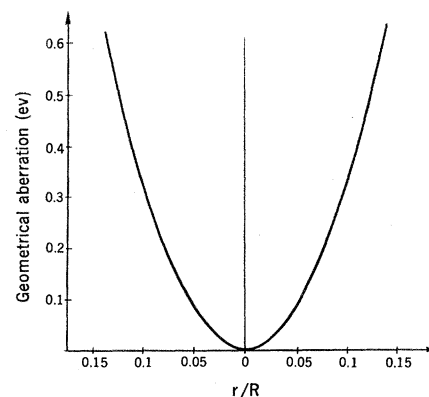


Fig. 3. Geometrical aberration of a spherically bent crystal versus the ratio of the radius of curvature ( $r$ ) to the diameter of the Rowland circle ( $R$ ). Diffraction of  $\text{AlK}\alpha$  radiation from Y-cut quartz (01  $\cdot$  0).

monochromator. The  $AlK\alpha$  x-ray line is focused onto an arc of the Rowland circle and irradiates the sample. The energy of the incident photons varies across the sample by about 1 electron volt, which is the width of the x-ray line. Consequently, the photoelectrons from a given energy level will also have energies which vary by 1 electron volt across the sample.

The electrons from the sample will, in general, come from many energy levels and hence may have energies ranging from 0 to 1487 electron volts, the upper limit being the energy of the incident photons. The electrons enter an electrostatic lens system which focuses the photoelectrons on the entrance aperture of the electron spectrometer and decelerates them to 115 electron volts. The electron spectrometer is normally adjusted to pass electrons with energies between 110 and 120 electron volts.

The four-element lens system was designed with sufficient degrees of freedom to provide the required deceleration, focusing of the sample on the electron spectrometer, and constant magnification. Incident electrons with energies from 300 to 1487 electron volts can be decelerated into the electron spectrometer passband and, at the same time, focused into an image of the sample at the entrance to the spectrometer. The size of this image is made independent of the incident electron energy (magnification, about 5), making possible dispersion compensation for all energies. The 1.0-electron volt spread in the energy of the photoelectrons across the sample from a single energy level is preserved in the image of the sample upon the input aperture of the electron spectrometer. The lens has been designed to minimize chromatic and spherical aberrations and to maximize intensity.

There is a set of field-terminating electrodes at the entrance to the spectrometer which is omitted from Fig. 1 for the sake of simplicity. The electrons enter a hemispherical electrostatic spectrometer with a central radius of 15.5 centimeters. This type of spectrometer was first analyzed by Purcell (6). At the exit plane of the spectrometer the electrons are focused onto an array of parallel lines, each line consisting of electrons coming from a particular energy level in the sample. Here they are detected by a multichannel electron multiplier device which will be described in more detail later. The amplified pulse resulting from each inci-

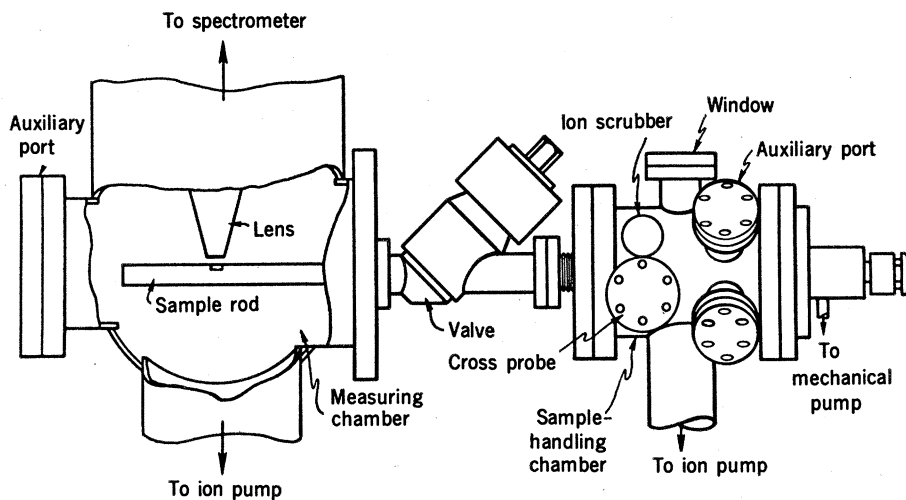


Fig. 4. Sample inlet system.

dent electron is fed into a multichannel analyzer or into the memory of a computer for further analysis. In order to obtain adequate shielding of the electron optical system from external fields, the spectrometer is surrounded by three concentric Mu-metal shields (nickel-iron alloy, 77 percent nickel and 16 percent iron) which reduce the magnetic field in the electron spectrometer to a level of about  $10^{-4}$  gauss.

#### Attainment of Higher Resolution

The various geometrical and electrical parameters of the system can be chosen so that the 1-electron volt width of the x-ray line does not contribute to the width of the electron lines at the

exit plane of the spectrometer. This is done by making the dispersion of the lens-spectrometer combination for the electrons equal in magnitude and opposite in sign to the dispersion of the crystal monochromator for the x-radiation, so that they cancel. This principle, known as dispersion compensation, is illustrated by the rays drawn in Fig. 1. The rays drawn through the lens and spectrometer represent photoelectrons ejected from a single energy level in the target. In the field-free region just outside the spectrometer their energy varies from  $(E - \Delta E)$  near the inner sphere to  $(E + \Delta E)$  near the outer sphere. Typically,  $E$  is between 110 and 120 electron volts, and  $\Delta E = 0.5$  electron volt. The focusing and dispersing properties of the spec-

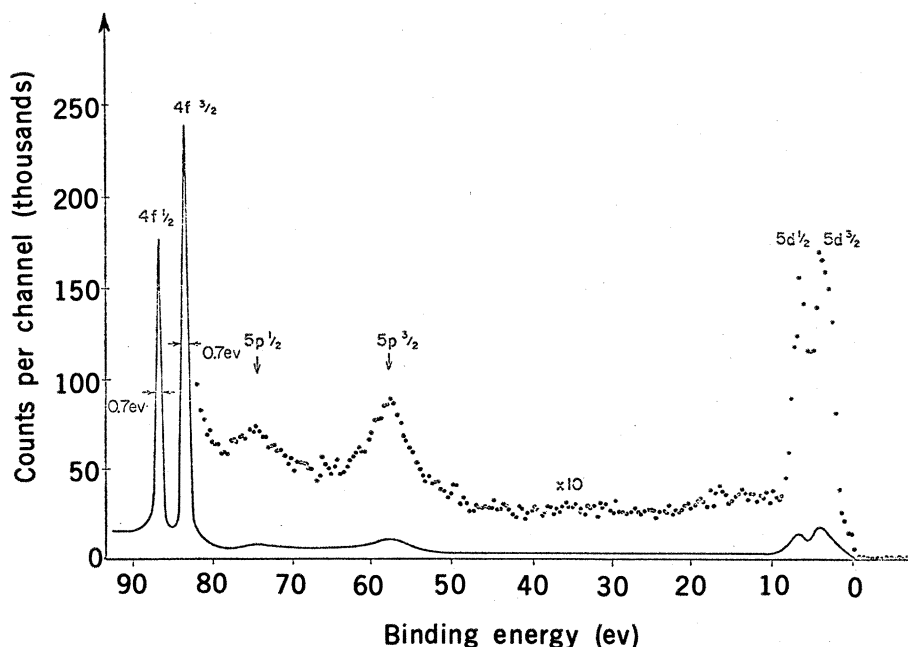


Fig. 5. The ESCA spectrum of gold obtained with monochromatized x-radiation: scanning time, 8 minutes; 1.5-kilowatt x-ray power; 2.5 channels per electron volt.

trometer bring these rays from a single energy level together into a line at the detector, the width of which, in principle, is independent of the inherent shape or width of the exciting radiation and the sample size, and is dependent only upon the energy level of the sample. Since no slits are used in this system, it operates always at maximum resolution and maximum sensitivity.

An alternative to the dispersion compensation method of achieving higher resolution is to introduce a slit between the x-ray monochromator and the target (2). The width of the slit can be made small relative to the x-ray line width on the Rowland circle such that one uses essentially monochromatic x-rays which do not contribute to the measured photoelectron line width. According to this approach, improved resolution is accompanied by a severe loss in intensity. In cases where dispersion compensation is difficult to achieve, as with solid samples of uneven surface or with gas samples, one can gain in intensity by using a concentrated source such as a rotating anode. With a rotating anode, one

can achieve power densities higher by an order of magnitude than can be achieved with stationary anodes. The spherically bent crystal focuses the radiation from a point source onto the sample with an energy which is monoenergetic within the resolution limits of the monochromator. However, with dispersion compensation, a surface roughness of several tenths of a millimeter will not appreciably degrade the resolution.

### Crystal Monochromator Design

Bent crystal x-ray monochromators have been used extensively for many years. To improve the resolution to better than the natural line width of the  $AlK\alpha$  emission line (0.9 electron volt at an incident photon energy of 1486 electron volts) requires a resolution substantially better than 1700 : 1, which necessitates the bending of the crystal atomic planes to optical wavelength accuracy. In order to collect as much x-ray intensity as possible, it is desirable to make the ratio of the crystal diameter to the radius of cur-

vature large within the limitations of geometrical aberrations. Cylindrically bent crystals, which are the easiest to make, have generally been used in the past. They have fairly poor x-ray collection efficiency. Spherically bent crystals are much better in this respect but are also very difficult to prepare with the required accuracy.

Figure 2 shows two views of the crystal monochromator. The plane of symmetry of the system, that is, the plane of Figs. 1 and 2A, passes through the center of one spherically bent quartz crystal. Two similar crystals are symmetrically positioned on either side of this plane, as shown in Fig. 2B.

The crystals, which are 3.5 centimeters in diameter, were formed from thin wafers having (in the unstressed condition) parallel plane surfaces cut on the  $(01 \cdot 0)$  crystal plane. After spherical bending, the concave surface on which the x-rays impinge is of optical quality and has a precise radius of curvature of 28 centimeters. Each crystal may be regarded as having a separate Rowland circle in a different plane from the others. These three planes intersect in the line passing through the anode and the sample, as shown in Fig. 2B.

The diameter of the Rowland circle is equal to the radius of curvature of the atomic planes of the bent crystal. This geometry introduces aberrations which limit the diameter of the reflecting crystal (see Fig. 3).

The reflection of the  $AlK\alpha$  radiation from the  $(01 \cdot 0)$  crystal planes takes place at a Bragg angle  $\theta$  of  $78.5^\circ$ . A Bragg angle close to  $90^\circ$  has the advantages of minimizing the geometrical aberrations and maximizing the Bragg diffraction intensity and the dispersion of the monochromator.

The bending of each crystal wafer causes it to have a nonuniform strain distribution and hence a variation in lattice spacing throughout the wafer. This variation of lattice spacing in the thin surface layer (3 micrometers) which the x-rays penetrate gives rise to a significant aberration. However, this aberration has the opposite sign from that of the geometrical aberration resulting from the lack of conformation of the crystal surface to the Rowland circle, so that they partially cancel. By proper choice of wafer thickness and other parameters, a considerable degree of cancellation has been attained.

The resolution of the monochroma-

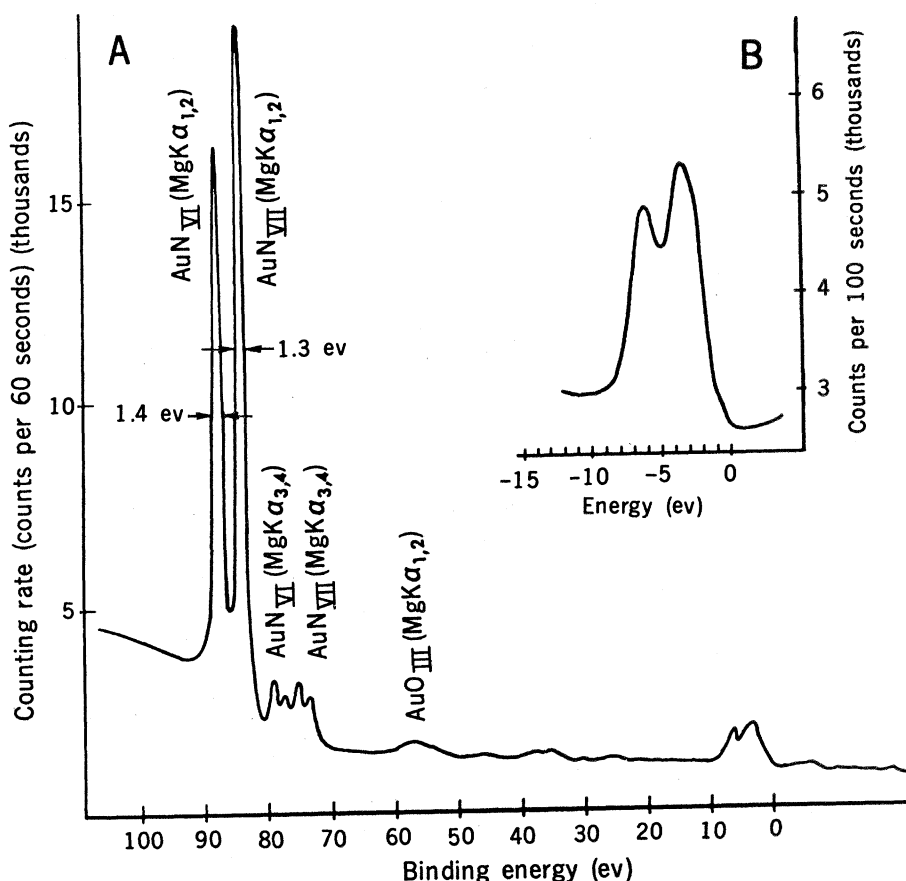


Fig. 6. (A) The ESCA spectrum of gold obtained with unmonochromatized x-radiation: the  $O_{1s}$  peak is obscured by satellite radiation from the  $K\alpha_{3,4}$  line of the x-ray source (1). (B) The ESCA spectrum of the valence band of gold at  $510^\circ C$ .

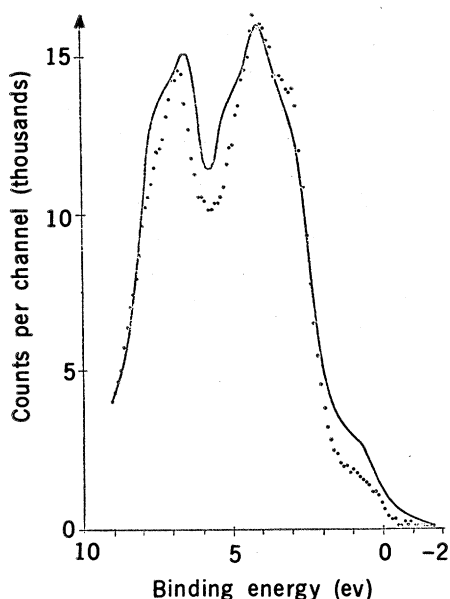


Fig. 7. Valence band of gold: scanning time, 15 minutes; 1.5 kilowatt x-ray power. (Dotted line) Experimental curve; (solid line) theoretical band structure curve from (9), with contribution due to scattered electrons added.

tor is determined partly by these aberrations but also partly by the inherent resolution resulting from the finite number of atomic planes involved in the Bragg diffraction. This inherent resolution has been computed theoretically to be 0.16 electron volt, and this value has been verified experimentally. With aberration effects included, the total resolution of the monochromator has been estimated to be about 0.20 electron volt, a value in agreement with experimental data. Measurements of the resolution of the lens and electron spectrometer made with a thermal source give a resolution of 0.25 electron volt. The minimum electron line width observed with the assembled ESCA system is about 0.5 electron volt, which probably is limited by the inherent width of the atomic energy level.

### Detection System

At the exit plane of the spectrometer the electrons impinge on a multichannel electron multiplier. It consists of an array of  $167 \times 32$  individual electron multipliers, each with a gain of about  $10^7$ . The long dimension of the array (2.5 centimeters) is in the radial direction of the spectrometer. A 10-electron volt range of electron energies is detected simultaneously. The spacing of the detector elements, therefore,

contributes  $10 \text{ electron volts}/167 = 0.06 \text{ electron volt}$  to the resolution, an amount that is small in comparison with other factors.

Each electron incident on the multiplier generates an amplified pulse of electrons on the output side which is then accelerated onto a phosphor screen, creating a pulse of light. These light pulses are imaged onto the photosensitive layer of a Vidicon camera where they are transformed into localized electrical charges. These are temporarily stored until the Vidicon electron beam scans across the signal and converts them into electrical pulses at the output. Thus, all electrons arriving at the detector at any energy and at any time are detected and the events are stored in the Vidicon memory until the signal is transferred to the core memory of a multichannel analyzer with a channel memory resolution of  $10^6$ . The multichannel analyzer also monitors the scan voltage of the Vidicon camera, from which it derives the information necessary to sort the pulses into 128 memory channels according to the energies of the electrons. Electrons from an arbitrarily wide range of initial energies can be counted by sweeping the lens electrode voltages and applying an appropriate swept voltage to the multichannel analyzer. The simultaneous detection of electrons in 128 resolvable elements over a 10-electron volt range results in a 128:1 increase in the rate of information acquisition over that of conventional detection systems in which a single slit giving comparable resolution and an electron multiplier are used.

### Inlet System Design

Figure 4 shows the inlet system of the instrument. The sample is mounted on a sample rod, which is shown in its fully inserted position. The sample is then positioned in the measuring chamber so that a 1- by 5-millimeter area is illuminated by  $\text{AlK}\alpha$  x-rays. Photoelectrons generated enter the lens immediately above the sample.

A valve separates the measuring chamber from the sample-handling chamber. With samples having low vapor pressure, a pressure of  $10^{-9}$  torr has been obtained in the measuring chamber. By inserting the sample rod about one-third of its length, the sample can be brought to the center of the sam-

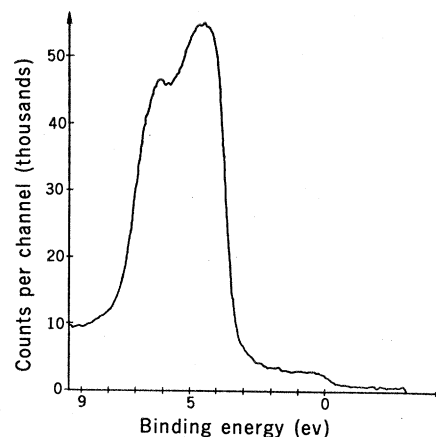


Fig. 8. Valence band of silver.

ple-handling chamber. Here the sample can be subjected to a variety of treatments. Gas can be let in through a valve to be adsorbed by the sample. The clean sample surfaces can be prepared by ion bombardment with a specific ion beam. A thin layer of material can be deposited on the target by means of an evaporator introduced through a cross probe. A pressure of the order of  $10^{-6}$  torr can be maintained during this deposition process, resulting in a clean sample surface.

The sample-handling chamber is separated from the outside by a pair of differentially pumped seals. With the sample rod pulled out far enough to permit samples to be loaded from the outside, the sample-handling chamber is still evacuated.

### System Optimization

The monochromator, lens, electron spectrometer, and detector form a system which has to be optimized for maximum intensity. The power loss in the ESCA system is extreme; typically, for an input power of about 1 kilowatt a few thousand electrons per second arrive at the detector. The input power is limited by the power density which can be dissipated at the anode and can be utilized to illuminate the sample. The efficiency of the monochromator depends on the width of the x-ray line (1 electron volt for  $\text{AlK}\alpha$ ); the dispersion (which is a maximum for large Bragg angles and a large diameter of the Rowland circle); and the resolution, diffraction efficiency, and acceptance angle of the reflecting crystals. It is limited by the physical size and the maximum possible bending of the crystals and the geometrical

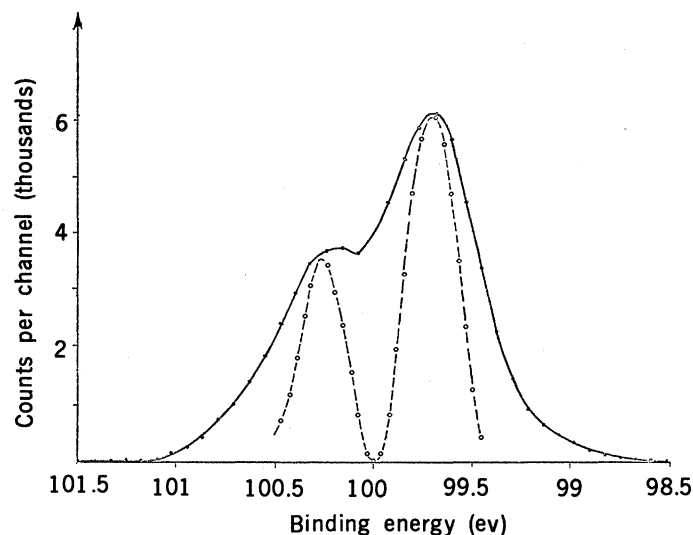
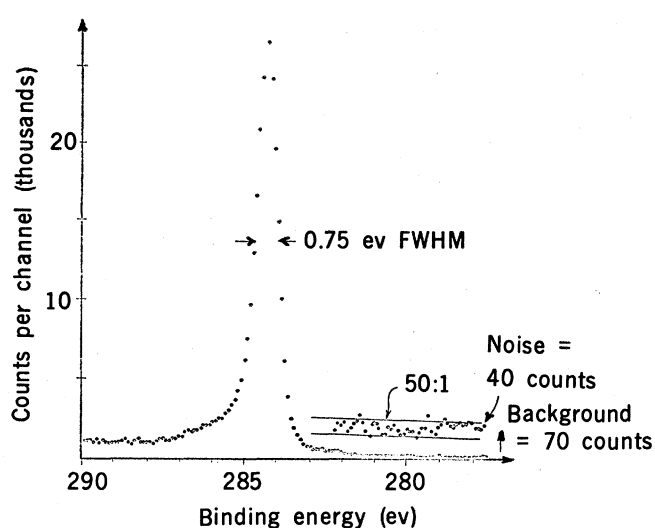


Fig. 9 (left). Carbon  $1s$  line: scanning time 5 minutes; 0.75-kilowatt x-ray power; 10 channels per electron volt. Fig. 10 (right). (Solid line) Silicon  $2p$  doublet ( $L_{II}$  and  $L_{III}$  subshells): scanning time, 100 seconds; 1.5-kilowatt x-ray power; (dashed line) deconvolution with a Gaussian line shape of 0.4 electron volt FWHM.

aberrations. The étendue (object size multiplied by the acceptance angle) of the lens and electron spectrometer is mainly influenced by aberrations (7) and by dispersion compensation, which requires a certain fixed ratio of object to image size produced by the lens. A larger physical size of the lens and the electron spectrometer permits collection of electrons from a larger object, thus making possible a greater étendue; the size of the instrument will be limited mainly by practical considerations, such as machinability and portability. Finally, the spatial resolution of the multichannel detector has to be high enough so as not to degrade the output resolution of the spectrometer.

### Experimental Results

Figure 5 shows an electron spectrum of the outer levels of gold, including the  $4f$  doublet ( $N_{VI}$  and  $N_{VII}$  subshells); 256 memory channels of the multichannel analyzer were used over a 100-electron volt range, giving approximately 0.4 electron volt per channel. To obtain the spectrum, the 10-electron volt simultaneous detection window was swept repeatedly over the 100-electron volt range for 8 minutes. The region to the right of the  $4f$  doublet is plotted on a vertical scale expanded ten times.

For comparison, the same spectrum, this time obtained without monochromatization of the x-rays, is shown in Fig. 6. Monochromatization removes

the  $4f$  satellite lines resulting from the  $AlK\alpha_{3,4}$  doublet, revealing clearly the  $Au5p\frac{1}{2}$  ( $O_{II}$  subshell) line in Fig. 5, which is obscured by satellite radiation from the  $K\alpha_{3,4}$  line in Fig. 6. Background counts resulting from bremsstrahlung have also been removed. The remaining background in the neighborhood of the  $5p$  lines consists of electrons from the conduction band which have lost energy in emerging from the sample.

The energy levels should be referenced to the Fermi level, and it would be desirable if the position of the Fermi level could be measured by the same method to avoid systematic errors. This is possible for a number of elements such as the noble metals. In Fig. 7, which shows the valence band of gold, there are two peaks of the  $5d$  doublet with a very distinct step at the side characterized by low binding energy. This step results from the (overlapping)  $6s$  and  $6p$  levels which are only partially filled. Therefore, at the Fermi level the electron density drops to zero within the range of thermal energies of the electrons, which is about  $1 kT$  ( $k$  is the Boltzmann constant and  $T$  is the absolute temperature) or 25 millielectron volts. With the high-resolution ESCA system this step can be measured and thus an absolute scale established. Furthermore, with monochromatized x-rays the background above the Fermi level drops virtually to zero (about 100 counts due to detector noise) which aids in determining the position of the Fermi level. In ESCA measurements with

unmonochromatized radiation this step is spread over a wider energy range and becomes almost unrecognizable (8). The agreement (Fig. 7) between the experimental curve (dotted line) and the theoretically predicted one (solid line) (9) is quite remarkable. The contribution of scattered electrons has been added to the shape of the theoretically predicted line.

The valence band of silver is given in Fig. 8. Here the Fermi level is shown even more clearly since it is farther removed from the edge of the valence band.

Two basic tests of the performance of any ESCA system may be made: one defines sensitivity, and the other, resolution. Graphite is a convenient sample for the first test. Figure 9 shows the carbon  $1s$  line. The power input to the x-ray source was 0.75 kilowatt. A region 12.5 electron volts wide was scanned repeatedly for 5 minutes with the use of 128 memory channels. The peak height is about 26,500 counts, the signal-to-noise ratio is 660, and the signal-to-background ratio is 380. The full line width at half-maximum height (FWHM) is 0.75 electron volt. For this test both the absolute peak height, which is uncertain owing to statistical variations, and the signal-to-noise ratio, obtained during a given measurement time, are important. The statistical variation of the peak height is  $\pm 490$  counts for three times the standard deviation, and the background noise contributes an additional 40 counts. This test is equally valid for instruments which do not

accumulate data simultaneously in 128 channels but use a single slit which is gradually moved across the spectrum. For such a slit system to obtain the same total peak count, an accumulation rate that is 128 times faster is required.

The best estimate thus far of system resolution has been made by means of the silicon  $2p$  doublet spectrum, which is shown in Fig. 10, after the contribution due to scattered electrons has been subtracted. The two components of the doublet, which are known to be separated by 0.6 electron volt (10), are partially resolved. A deconvolution with a Gaussian line shape of 0.4 electron volt FWHM has been used to separate the components (dashed line). The vertical scale of the deconvolved curve has been reduced to fit under the experimental one. The width of the two deconvolved lines is 0.3 electron volt.

Recent work by Gaehwiller and Brown (10) in ultraviolet absorption spectroscopy has shown that the  $2p\ 1/2$  and  $2p\ 3/2$  ( $L_{II}$  and  $L_{III}$  subshells) absorption edges of silicon are extremely sharp, ranging from 0.03 to 0.1 electron volt for different materials. Unfortunately, these measurements were made on samples about 3000 angstroms thick, whereas typical ESCA electrons originate from less than 50 angstroms below the surface of a solid sample. Therefore, because of possible surface effects, the measurements of absorption edges can be applied only with caution to the ESCA case. Nevertheless, they are an indication that a silicon sample can be used as a standard for a resolution test in the ESCA system.

Figure 11 shows another spectrum of silicon, scanned over a 100-electron volt range for 5 hours and stored in 256 memory channels. The  $2p$  doublet (not resolved in this case) and the  $2s$  lines are shown. Each is accompanied by a satellite on the high-binding-energy side resulting from the partial oxidation of the sample. From ellipsometric measurements on silicon (11), it has been shown that an oxide layer a few atomic layers thick forms at the surface within a short time after exposure of the element to air. This very thin layer can easily be recognized by ESCA measurements. Furthermore, from the magnitude of the chemical shift (3.8 and 3.9 electron volts) we know that this oxide layer consists predominantly of silicon dioxide. Finally, there is very little difference in

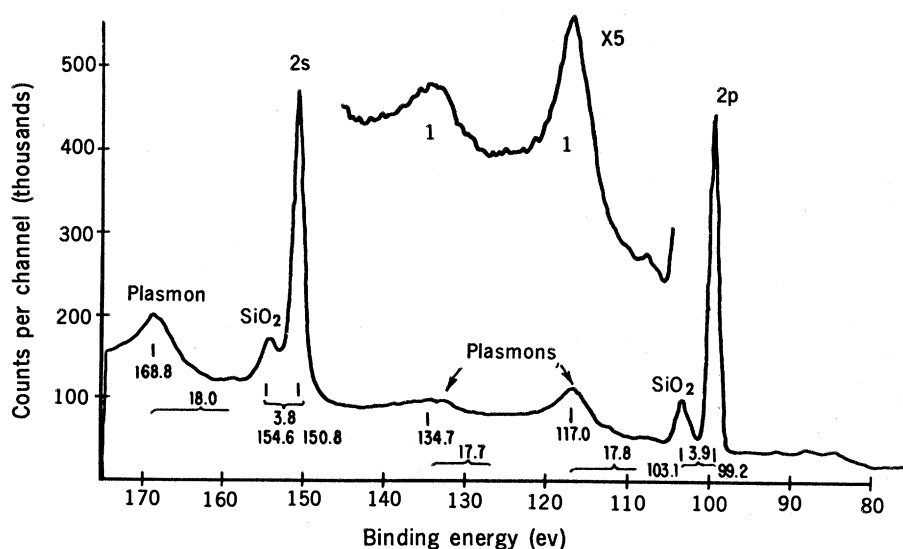


Fig. 11. The ESCA spectrum of silicon showing surface oxide layer and first- and second-order plasmons.

the chemical shift of the  $2s$  and  $2p$  levels.

The two smaller peaks at binding energies of 117.0 and 134.7 electron volts are plasmon resonances scattered from the  $2p$  line. Plasmon resonances are oscillations of the electron gas (plasma) in the conduction band of the metal or semiconductor, excited by the escaping photoelectrons. When the photoelectron excites the plasma, it loses energy in discrete amounts. The plasmon lines are separated from the  $2p$  line by  $17.8 \pm 0.5$  and  $35.5 \pm 1.0$  electron volts. A plasmon resonance scattered from the  $2s$  line should have the same shift in energy as one scattered from the  $2p$  line. The measured value is  $18.0 \pm 0.5$  electron volts.

Another example of the sensitivity obtainable with the ESCA system is given in Fig. 12. In this case a thin film of antimony was evaporated in situ, and the spectrum was measured (curve 1). The antimony was then exposed to air for 20 minutes, and

then the spectrum was measured again (curve 2). The new peaks observed result from antimony oxide. Thus, one can investigate surface reaction kinetics and can determine the binding state of the reaction products from the shift in binding energy. This spectrum also shows a rare coincidence of two ESCA lines. The ratio of the peak height of the antimony-antimony oxide lines is different for the  $3/2$  and the  $5/2$  line. It turns out that the oxygen  $1s$  line lies at 532 electron volts and, therefore, contributes to the  $5/2$  line of antimony oxide. Generally, it is very simple to switch to another line which is free of interferences, in this case, the  $3/2$  line.

## Conclusions

Electron spectroscopy for chemical analysis is being used today in many laboratories for a wide range of applications. They include investigations of

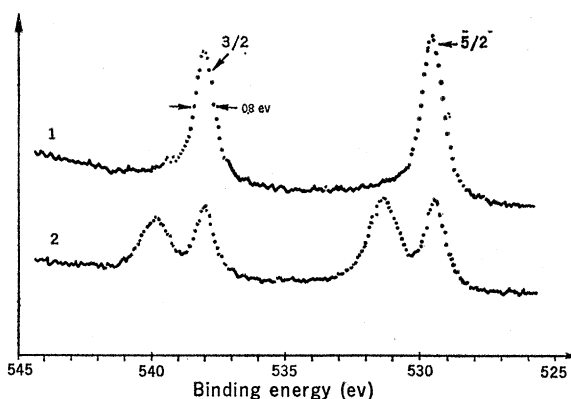


Fig. 12. The ESCA spectrum of antimony. Curve 1, antimony evaporated in situ; curve 2, partially oxidized antimony after exposure to air for 20 minutes.

the band structure of crystals, the binding state of atoms in chemical compounds, surface chemistry and surface physics, particularly catalysis and adsorption phenomena, and elemental analysis and structural analysis of chemical substances, to mention a few. The use of monochromatized x-radiation results in improved resolution and the freedom from satellites. The reduced background improves the information content of the ESCA spectra significantly. Often, the actual shape of the ESCA line or the energy band becomes more clearly visible since it is less distorted by instrumental

line shape. The signal-to-noise ratio is significantly improved and the instrumental background is purely statistical and independent of energy. Thus, the instrumental background does not introduce any structure into the ESCA spectrum which could be mistaken for actual information.

#### References and Notes

1. K. Siegbahn *et al.*, *ESCA, Atomic, Molecular and Solid State Structure Studied by Means of Electron Spectroscopy* (Almqvist & Wiksells, Uppsala, 1967).
2. K. Siegbahn *et al.*, *ESCA Applied to Free Molecules* (North-Holland, Amsterdam and London, 1970).
3. D. W. Turner, C. Baker, A. D. Baker, C. R. Brundle, *Molecular Photoelectron Spectroscopy* (Interscience, London, 1970).

4. L. G. Parratt, *Rev. Mod. Phys.* **31**, 616 (1959).
5. A. Fahlman and K. Siegbahn, *Ark. Fys.* **32**, 111 (1966).
6. E. M. Purcell, *Phys. Rev.* **54**, 818 (1938).
7. J. C. Helmer and N. H. Weichert, *Appl. Phys. Lett.* **13** (No. 8), 266 (1968).
8. Y. Baer, P. F. Hedén, J. Hedman, M. Klas-son, C. Nordling, K. Siegbahn, *Phys. Scr.* **1**, 55 (1970).
9. N. V. Smith and M. M. Traum, paper presented at the International Conference on Electron Spectroscopy, Pacific Grove, Calif., 1971.
10. C. Gaehwiller and F. C. Brown, paper presented at the Conference on the Physics of Semiconductors, Cambridge, Mass., 17-22 Aug. 1970.
11. R. J. Archer, *J. Electrochem. Soc.* **104**, 619 (1957).
12. Many people have contributed significantly to the design of this instrument, among them R. Moody, H. Weaver, A. Melera, and C. Tyler.

## Fast Transport of Materials in Mammalian Nerve Fibers

A fast transport mechanism for materials exists in nerve fibers, which depends on oxidative metabolism.

Sidney Ochs

Since Waller's demonstration in 1850 that nerve fibers distal to a transection undergo a typical sequence of degenerative changes, the suggestion has been advanced that materials needed to maintain the viability of axons are being continually supplied from their cell bodies (1). Within the last several decades evidence for a slow transport of material in nerve fibers at a rate of 1 to 10 millimeters per day has accumulated, initially on the basis of damming, and subsequently by the use of isotope tracer techniques (2). Only within the last several years have much faster transport rates been reported (3). If one considers that Wallerian degeneration makes its appearance only a few days after nerve section and that it occurs over relatively long lengths of nerve, a fast transport system would be required to provide a continuous supply of the substances postulated to keep

the nerve fibers viable. However, there has been some uncertainty regarding the rate of fast transport, with reported values ranging from 50 to over 2000 mm/day (3). The values obtained depend in part on which technique is used for rate determination, whether it is by measurement of accumulated proteins labeled with radioisotopes, transmitter substances at a ligation or at the nerve ending, or by determination of the pattern of outflow of labeled materials in the nerve. The values also depend on whether mammalian or nonmammalian nerves are studied. In general, slower rates are found in invertebrate nerves. In any event, the variations found within a given species or even in the nerves of the same animal, have suggested to some the possibility that the rate might depend on the physiological state of the nerve or that more than one fast transport system is present in the nerve fiber.

Recently, a well-defined fast transport system was described with a rate close

to  $400 \pm 35$  (S.D.) mm/day (4, 5). This was shown in cat sciatic nerve by the appearance of a crest of activity from labeled proteins passing down the axons after the amino acid precursor [ $^3\text{H}$ ]leucine had been injected into the cell bodies of the lumbar 7th (L7) dorsal root ganglia or into the motoneurons of the L7 segment of the spinal cord. In this article the characteristic properties of this fast transport system in the mammal are described; reference to studies made in nonmammalian species can be found in recent reviews (2, 3).

The fast transport system in the mammalian nerve indicated by the downward flow of a crest of radioactivity also occurs in vitro. This finding allowed further studies to be made of the nature of the underlying mechanism, and it was subsequently discovered that fast axoplasmic transport depends upon oxidative phosphorylation, with adenosine triphosphate (ATP) supplying energy to the transport mechanism locally in the axon. These results led to a "transport filament" model for fast axoplasmic transport which is described herein.

### The Generality of Fast Axoplasmic Transport

Figure 1 shows the pattern of fast transport in sciatic nerves taken from cats at different intervals after injecting [ $^3\text{H}$ ]leucine into the L7 dorsal root ganglia. The ganglia remain highly radioactive throughout, and after approximately 2½ to 3 hours, a plateau of activity appears in the nerve distal to the ganglia. More distally, the activity rises to a crest before falling abruptly to the baseline. As is described later, the

The author is in the department of physiology, Indiana University Medical Center, Indianapolis 46202.